PHYSICAL REVIEW D VOLUME 23, NUMBER 11 1 JUNE 1981

Parton and valon distributions in the nucleon

Rudolph C. Hwa and M. Sajjad Zahir
Institute of Theoretical Science and Department of Physics, University of Oregon, Eugene, Oregon 97403
(Received 17 June 1980; revised manuscript received 16 September 1980)

Structure functions of the nucleon are analyzed in the valon model in which a nucleon is assumed to be a bound state of three valence quark clusters (valons). At high Q^2 the structure of the valons is described by leading-order results in the perturbative quantum chromodynamics. From the experimental data on deep-inelastic scattering off protons and neutrons, the flavor-dependent valon distributions in the nucleon are determined. Predictions for the parton distributions are then made for high Q^2 without guesses concerning the quark and gluon distributions at low Q^2. The sea-quark and gluon distributions are found to have a sharp peak at very small x. Convenient parametrization is provided which interpolates between different numbers of flavors.

I. INTRODUCTION

Any determination of parton distributions in a nucleon in the framework of quantum chromodynamics (QCD) always involves some model-dependent procedure. For example, Buras and Gaemers[1] considered only the $n=2$ and 3 moments to obtain parametrizations of sea-quark and gluon distributions in the region $x<0.3$. Owens and Reya[2] assumed some simple and smooth functions for the sea-quark and gluon distributions for all x at some low Q^2, and obtained rather different results from Ref. 1 at high Q^2. Our procedure in this paper will likewise depend on a model. Instead of relying on mathematical simplicity as a guide, we shall emphasize the physical picture for nucleon structure. That is, we require that our model for the nucleon be compatible with the description of the bound-state problem in terms of three constituent quarks. In order to emphasize that in the scattering problem these constituents should be regarded as valence quark clusters rather than pointlike objects, they have been referred to as valons.[3,4]

Recent development in the subject of parton distributions has been in the direction of including contributions from nonleading terms in asymptotic freedom or target-mass effects.[5-8] It extends the validity of the theory to lower values of Q^2 and therefore facilitates more reasonable comparisons with data at low Q^2. Our effort is aimed in a different direction. We use data only at high Q^2 where the leading-order approximation is good. Our improvement is in the physical content of the model by which parton distributions are extracted from structure functions. An equally important objective in this paper is to determine the nucleon wave function in terms of the valons. The momentum distribution of the valons in a nucleon summarizes the bound-state complications due to confinement so that once known, albeit phenomenologically, certain difficult aspects in the treatment of hadronic (hard or soft) processes, such as hadronization, can be alleviated. A rough knowledge of the flavor-independent valon distribution has already been applied to the determination of quark and gluon decay functions and low-p_T inclusive cross sections with great success.[4,9] In this paper we do a more thorough analysis of the deep-inelastic scattering data and determine the flavor-dependent valon distributions.

The concept of using constituent quarks as an intermediate step between hadron and current quarks is not new.[10] The procedure followed in this paper shares a common basis with the method used by Glück and Reya,[10] except that we emphasize more the physical implications. Moreover, due to the inadequacy of data their analysis was performed for a value of Q^2 (3 GeV^2) at which the leading-order approximation is invalid. In addition, the value of strong-interaction scale parameter Λ was guessed. In this paper we shall use both muon and neutrino scattering data for $Q^2 > 20$ GeV^2 as phenomenological input. We shall show that the data are compatible not only with QCD but also with the valon model. After determining the valon distribution, we calculate uniquely the quark and gluon distributions. The results are presented in terms of simple parametric forms which are useful for theoretical and experimental applications to many reactions involving the nucleon.

II. NUCLEON STRUCTURE

Recent investigations in the subject of nucleon structure have mainly been in two opposite directions. On the one hand, one studies the bound state in terms of three quarks, such as in a bag model, and obtains various static properties of the nucleon and its spectroscopic partners. On the other hand, one probes the nucleon with high-energy leptons in the hope of learning something

about the three constituent quarks but finds structure functions that can only be understood in terms of an infinite number of partons (i.e., quarks, antiquarks, and gluons). The two views can be reconciled if we recognize that the constituents in the quark model for the static nucleon are not the same objects as the quarks in the parton model. Since the scales of spatial resolution are different for the two problems, we may regard the former as clusters of the latter without contradicting either view. The clusters have quantum numbers of the valence quarks, and have been called valons, for short.[3,4]

In static problems there is little difference between the usual constituent quarks and the valons, since the pointlike nature of the constituent quarks is not a crucial aspect of the description, and has been assumed mainly for simplicity. But in scattering problems it is important to recognize that the valons are different from point quarks because the valons, being clusters of partons, cannot easily undergo scattering as a whole. Stated differently, the virtual emission and absorption of gluons in a valon become bremsstrahlung and pair creation processes under scattering, since energy is available to make virtual processes real.

The fact that the bound-state problem of the nucleon can be well described by three constituent quarks implies that the spatial extensions of the valons do not overlap appreciably. A physical picture of the nucleon in terms of three valons is then quite analogous to the usual picture of a deuteron in terms of two nucleons. At low Q^2 the resolution is low and the description of the deuteron as a bound state of two nucleons is adequate. The medium-to-long-range part of the deuteron wave function summarizes the bound-state problem. In that description it is not necessary to introduce the pion as a third constituent, even though it is the exchange of pions that effects the binding. The short-range part of the deuteron wave function is complicated and is intimately related to the nucleon structure. Indeed, at high Q^2 we are able to resolve the constituents of the nucleons, the momentum distribution of which is minimally affected by the spectator nucleon in the deuteron. The deuteron wave function plays only the role of smearing the nucleon structure functions to account for the Fermi motion of the nucleons in the deuteron. These familiar statements about the deuteron are made at length here for the purpose of providing an insight into our description about the nucleon in terms of the valons. Exact analogy is attained by substituting nucleon for deuteron, and valons for nucleons.

Let $\mathcal{F}^N(x,Q^2)$ be a structure function (e.g., F_2 or xF_3) of the nucleon, and $\mathcal{F}^v(z,Q^2)$ be the corresponding function of a valon v. According to the above description of our model of the nucleon, the two functions are related by a smearing of the valon momentum in the nucleon, i.e.,

$$\mathcal{F}^N(x,Q^2)=\sum_v \int_x^1 dy\, G_{v/N}(y)\mathcal{F}^v(x/y,Q^2)\,, \quad (2.1)$$

where $G_{v/N}(y)$ is the probability for the valon v to have momentum fraction y in the nucleon and the summation is over the three valons. In analogy to the deuteron example we ignore the gluons that bind the valons. We shall also assume that the three valons carry all the momentum of the nucleon. The implication is that the exchange of very soft gluons is responsible for the binding, as is reasonable. Involved in (2.1) is also the assumption that in deep-inelastic scattering at high Q^2 the valons are independently probed, since the shortness of interaction time makes it reasonable to ignore the response of the spectator valons. Thus through (2.1) we have broken up the hadron structure problem into two parts. One part represented by $G_{v/N}(y)$ describes the wave function of the nucleon in the valon representation. It contains all the hadronic complication due to confinement. It is independent of Q^2 or the probe. The other part represented by $\mathcal{F}^v(z,Q^2)$ describes the virtual QCD processes of gluon emission and quark-pair creation. It refers to an individual valon independent of the other valons in the nucleon and consequently also independent of the confinement problem. It depends on Q^2 and the nature of the probe.

At sufficiently high Q^2, $\mathcal{F}^v(z,Q^2)$ can be described accurately by the leading-order result in QCD. Its moments can be expressed completely in terms of the evolution parameter

$$s=\ln\frac{\ln Q^2/\Lambda^2}{\ln Q_0^2/\Lambda^2}\,, \quad (2.2)$$

where Λ and Q_0 are scale parameters to be determined by experiments. We assume that Λ and Q_0 are independent of the order n of the moments. From the theoretical standpoint this assumption is strictly incorrect, if nonleading contributions are to be represented by an effective Λ.[11] However, on the one hand there are other contributions (e.g., target-mass effects) which add uncertainties to the clean theoretical predictions of perturbative QCD, while on the other hand experimental data are not of such precision as to invalidata an n-independent Λ parametrization. Since the key inputs in this work are high-Q^2 data and leading-order QCD, both of which are consistent with Λ being independent of n, we shall do phenomenolgoy with complete neglect of the high-order

effects.

Before the precise expressions for $\mathcal{F}^v(z,Q^2)$ are exhibited, we note first that it has the property that it becomes $\delta(z-1)$ as Q^2 is extrapolated to ${Q_0}^2$ (beyond the region of validity). This mathematical boundary condition signifies that the internal structure of a valon cannot be resolved at Q_0 in the (unrealistic) leading-order approximation. Accordingly, when this property is applied to (2.1), the structure function of the nucleon becomes directly related to $xG_{v/N}(x)$ at Q_0. That is, Q_0 is the effective value (defined by leading-order extrapolation) at which the nucleon may be regarded as consisting only of three valons. If a more accurate approximation scheme is used for extrapolation, one would probably arrive at a different numerical value for Q_0 at which the valon representation of the nucleon wave function is defined. The valon distribution $G_{v/N}(x)$ itself should not depend upon the extrapolation scheme if the model is a reasonable approximation of the physical reality, since the essence of the model is to regard the bound-state problem of the hadron as being separable from the internal-structure problem of the constituents. Indeed, $G_{v/N}(x)$ should ultimately be determined theoretically by solving the bound-state problem independent of $\mathcal{F}^v(z,Q^2)$. In this paper we determine it phenomenologically using deep-inelastic scattering data at high Q^2.

Having stated the physical basis of our approach we proceed to the quantitative description. Let us first consider the structure function $F_2(x,Q^2)$ for μ scattering. Let the indices U and D denote u- and d-type valons. For the values of Q^2 at which data will be analyzed, we assume that only three flavors ($f=3$) are relevant. Thus we have for the U-valon structure function $F_2^{\mu U}(z,Q^2)$:

$$F_2^{\mu U}=\tfrac{4}{9}z\,(G_{u/U}+G_{\bar{u}/U})+\tfrac{1}{9}z\,(G_{d/U}+G_{\bar{d}/U}+G_{s/U}+G_{\bar{s}/U})\,, \tag{2.3}$$

where in obvious notation the right-hand side involves the probability functions for quarks to have momentum fraction z in the U valon at Q^2. A similar expression holds also for the D valon. Denoting $G_{u/U}$ by G_f where the subscript f stands for favored (quark evolution) and all the other G functions in (2.3) by G_{uf} (uf standing for unfavored evolution whose universality is due to the flavor independence of the intermediary gluons), we have

$$F_2^{\mu U}(z,Q^2)=\tfrac{4}{9}z\,[G_f(z,Q^2)+2G_{uf}(z,Q^2)]\,, \tag{2.4a}$$

$$F_2^{\mu D}(z,Q^2)=\tfrac{1}{9}z\,[G_f(z,Q^2)+11G_{uf}(z,Q^2)]\,. \tag{2.4b}$$

The flavor-singlet (S) and -nonsinglet (NS) components are defined by

$$G^S=\sum_{i=1}^{f}(G_{q_i/v}+G_{\bar{q}_i/v})=G_f+(2f-1)G_{uf}\,, \tag{2.5a}$$

$$G^{NS}=\sum_{i=1}^{f}(G_{q_i/v}-G_{\bar{q}_i/v})=G_f-G_{uf}\,, \tag{2.5b}$$

so that by inverting we have

$$G_f=\frac{1}{2f}[G^S+(2f-1)G^{NS}]\,, \tag{2.6a}$$

$$G_{uf}=\frac{1}{2f}(G^S-G^{NS})\,. \tag{2.6b}$$

Applying these to (2.4) for $f=3$, we obtain

$$F_2^{\mu U}(z,Q^2)=\tfrac{2}{9}z[G^S(z,Q^2)+G^{NS}(z,Q^2)]\,, \tag{2.7a}$$

$$F_2^{\mu D}(z,Q^2)=\tfrac{1}{9}z[2G^S(z,Q^2)-G^{NS}(z,Q^2)]\,. \tag{2.7b}$$

For neutrino interactions via charged current (but assuming $\theta_C=0$) we have

$$F_2^{\nu U}(z,Q^2)=2z(G_{d/U}+G_{\bar{u}/U})=4zG_{uf}(z,Q^2)\,, \tag{2.8a}$$

$$\begin{aligned}F_2^{\bar{\nu}U}(z,Q^2)&=2z(G_{u/U}+G_{\bar{d}/U})\\&=2z[G_f(z,Q^2)+G_{uf}(z,Q^2)]\,,\end{aligned} \tag{2.8b}$$

while it is the other way around for νD and $\bar{\nu}D$ scattering. Using (2.6) again yields

$$\begin{aligned}F_2^{\nu U}(z,Q^2)&=F_2^{\bar{\nu}D}(z,Q^2)\\&=\tfrac{2}{3}z[G^S(z,Q^2)-G^{NS}(z,Q^2)]\,,\end{aligned} \tag{2.9a}$$

$$\begin{aligned}F_2^{\bar{\nu}U}(z,Q^2)&=F_2^{\nu D}(z,Q^2)\\&=\tfrac{2}{3}z[G^S(z,Q^2)+2G^{NS}(z,Q^2)]\,.\end{aligned} \tag{2.9b}$$

Similarly, one can obtain[3]

$$zF_3^{\nu U}(z,Q^2)=zF_3^{\bar{\nu}D}(z,Q^2)=0\,, \tag{2.10a}$$

$$zF_3^{\bar{\nu}U}(z,Q^2)=zF_3^{\nu D}(z,Q^2)=2zG^{NS}(z,Q^2)\,. \tag{2.10b}$$

Through (2.7), (2.9), and (2.10) all the structure functions of the valons have been expressed in terms of G^S and G^{NS}.

We now go to the moments of these distribution functions,[12] defining

$$M_{2,3}(n,Q^2)=\int_0^1 dx\,x^{n-2}\begin{Bmatrix}F_2\\xF_3\end{Bmatrix}(x,Q^2)\,, \tag{2.11}$$

$$M_\alpha(n,Q^2)=\int_0^1 dx\,x^{n-1}G_\alpha(x,Q^2),\quad \alpha=v/N,S,NS\,.$$

It then follows from (2.1) that (2.12)

$$M^N(n,Q^2)=\sum_v M_{v/N}(n)M^v(n,Q^2)\,. \tag{2.13}$$

In the following we shall always refer the valon distributions to those in the proton by charge symmetry, i.e.,

$$U(n)\equiv M_{U/p}(n)=M_{D/n}(n)\,, \tag{2.14a}$$

$$D(n)\equiv M_{D/p}(n)=M_{U/n}(n)\,. \tag{2.14b}$$

The number and momentum sum rules imply

$$U(1)=D(1)=1\,, \tag{2.15}$$

$$2U(2)+D(2)=1\,. \tag{2.16}$$

Now, for μ scattering we have from (2.7) and (2.13)

$$M_2^{\mu p}(n,Q^2)=\tfrac{2}{9}[2U(n)+D(n)]M^{S}(n,Q^2) + \tfrac{1}{9}[4U(n)-D(n)]M^{NS}(n,Q^2)\,, \tag{2.17a}$$

$$M_2^{\mu n}(n,Q^2)=\tfrac{2}{9}[2U(n)+D(n)]M^{S}(n,Q^2) - \tfrac{2}{9}[U(n)-D(n)]M^{NS}(n,Q^2)\,. \tag{2.17b}$$

For ν and $\bar{\nu}$ interactions we have, suppressing the n and Q^2 dependences,

$$M_2^{\nu p}=M_2^{\bar{\nu}n}=\tfrac{2}{3}(2U+D)M^{S}-\tfrac{4}{3}(U-D)M^{NS}\,, \tag{2.18a}$$

$$M_2^{\bar{\nu}p}=M_2^{\nu n}=\tfrac{2}{3}(2U+D)M^{S}+\tfrac{2}{3}(4U-D)M^{NS}\,, \tag{2.18b}$$

$$M_3^{\nu p}=M_3^{\bar{\nu}n}=2DM^{NS}\,, \tag{2.19a}$$

$$M_3^{\bar{\nu}p}=M_3^{\nu n}=4UM^{NS}\,, \tag{2.19b}$$

so for an average of ν and $\bar{\nu}$ interactions on an isoscalar target we obtain

$$M_2^{(\nu)}\equiv\tfrac{1}{4}(M_2^{\nu p}+M_2^{\nu n}+M_2^{\bar{\nu}p}+M_2^{\bar{\nu}n}) =\tfrac{1}{3}(2U+D)(2M^{S}+M^{NS})\,, \tag{2.20}$$

$$M_3\equiv\tfrac{1}{4}(M_3^{\nu p}+M_3^{\nu n}+M_3^{\bar{\nu}p}+M_3^{\bar{\nu}n}) =(2U+D)M^{NS}\,. \tag{2.21}$$

Equations (2.17), (2.20), and (2.21) form the basis of our phenomenological analysis of the nucleon structure functions. Note that the application of (2.16) to (2.20) and (2.21) yields, for $n=2$,

$$M_2^{(\nu)}(2,Q^2)=\tfrac{1}{3}[2M^{S}(2,Q^2)+M^{NS}(2,Q^2)]\,, \tag{2.22}$$

$$M_3(2,Q^2)=M^{NS}(2,Q^2)\,. \tag{2.23}$$

Thus the $n=2$ case offers direct relationships between the measurable quantities $M_2^{(\nu)}$, M_3 and the theoretical functions M^{S} and M^{NS} without any dependence on the valon distributions. Equation (2.23) has been exploited in Ref. 3 for the determination of Q_0.

For the moments of singlet and nonsinglet valon structure functions we shall use, as discussed earlier, the leading-order solutions of the renormalization-group equations in QCD. They can be expressed entirely in terms of the evolution parameter s. They are[13]

$$M^{NS}(n,Q^2)=\exp(-d_{NS}s)\,, \tag{2.24}$$

$$M^{S}(n,Q^2)=\tfrac{1}{2}(1+\rho)\exp(-d_{+}s) +\tfrac{1}{2}(1-\rho)\exp(-d_{-}s)\,, \tag{2.25}$$

where Q^2 and s are related by (2.2), and the anomalous dimensions d's and other associated parameters are

$$\rho=(d_{NS}-d_{gg})/\Delta\,,$$

$$\Delta=d_{+}-d_{-}=[(d_{NS}-d_{gg})^2+4d_{gQ}d_{Qg}]^{1/2}\,,$$

$$d_{NS}=\frac{1}{3\pi b}\left[1-\frac{2}{n(n+1)}+4\sum_{j=2}^{n}\frac{1}{j}\right],$$

$$d_{gQ}=\frac{-2}{3\pi b}\,\frac{2+n+n^2}{n(n^2-1)}\,,$$

$$d_{Qg}=\frac{-f}{2\pi b}\,\frac{2+n+n^2}{n(n+1)(n+2)}\,,$$

$$d_{gg}=\frac{-3}{\pi b}\left[-\frac{1}{12}+\frac{1}{n(n-1)}+\frac{1}{(n+1)(n+2)} -\frac{f}{18}-\sum_{j=2}^{n}\frac{1}{j}\right],$$

$$d_{\pm}=\tfrac{1}{2}[d_{NS}+d_{gg}\pm\Delta]\,,$$

$$b=(33-2f)/12\pi\,.$$

III. VALON DISTRIBUTIONS

The basic formalism of our model having been expressed for specific processes in (2.17), (2.20), and (2.21), we are now in a position to extract the valon distributions, or, more precisely, their moments $U(n)$ and $D(n)$. We use (2.24) and (2.25) for the nonsinglet structure functions of the valons, and we use experimental data at high Q^2 for the nucleon structure functions $M_2^{\mu p,n}$, $M_2^{(\nu)}$, and M_3. Evidently, the system of equations is highly constrained. In fact, we need only $M_2^{\mu p,n}$ at one value of Q^2 as phenomenological input; the neutrino data will actually be used to chek the predictions of our model.

To facilitate the phenomenological analysis, we assume a simple form for the exclusive valon distribution

$$G_{UUD/p}(y_1,y_2,y_3)=\alpha(y_1y_2)^{a}y_3^{b}\delta(y_1+y_2+y_3-1)\,, \tag{3.1}$$

where a and b are two free parameters, y_1 and y_2 refer to the two U valons, and y_3 refers to the D valon. Spin and color degrees of freedom have all been averaged over. The inclusive valon distributions can be obtained by double integration over the unspecified variables:

$$G_{U/p}(y)=\int dy_2dy_3G_{UUD/p}(y,y_2,y_3) =B(a+1,a+b+2)^{-1}y^{a}(1-y)^{a+b+1}\,, \tag{3.2}$$

$$G_{D/p}(y)=\int dy_1,dy_2G_{UUD/p}(y_1,y_2,y) =B(b+1,2a+2)^{-1}y^{b}(1-y)^{2a+1}\,. \tag{3.3}$$

The normalization parameter α has been fixed

by (2.15), i.e.,

$$\int_0^1 G_{U/p}(y)dy = \int_0^1 G_{D/p}(y)dy = 1 \tag{3.4}$$

and $B(\beta, \gamma)$ is the Euler beta function. The momentum sum rule (2.16) is automatically satisfied as can be verified since it is built in via the δ function in (3.1).

The moments of these inclusive valon distributions, according to (2.12) and (2.14), are therefore

$$U(n) = \frac{B(a+n, a+b+2)}{B(a+1, a+b+2)}, \tag{3.5a}$$

$$D(n) = \frac{B(b+n, 2a+2)}{B(b+1, 2a+2)}. \tag{3.5b}$$

For the data that we shall analyze, these two-parameter formulas will prove to be quite adequate.

For neutrino scattering off isoscaler targets, (2.20) and (2.21) reveal that the combination $2U + D$ is involved in both $M_2^{(\nu)}$ and M_3, so data on those structure functions alone cannot be used to resolve the U and D moments. Thus either $M_2^{\mu p}$ or $M_2^{\mu n}$ or both must also be used. Their moments are given by Duke and Roberts[14] whose analysis is based on the muon scattering data of the Chicago-Harvard-Illinois-Oxford (CHIO) collaboration[15] and the electron scattering data from SLAC.[16] The moments for the highest value of Q^2 (22.5 GeV^2) are determined mainly by the CHIO muon data. They are shown in Fig. 1. We have determined $U(n)$ and $D(n)$ by fitting $M_2^{\mu p}(n, Q^2)$ and $M_2^{\mu n}(n, Q^2)$ at $Q^2 = 22.5$ GeV^2 using (2.17) in conjunction with (2.24), (2.25), and (3.5). The following values of the parameters are obtained:

$$a = 0.65, \quad b = 0.35, \tag{3.6}$$

$$Q_0 = 0.81 \text{ GeV}, \quad \Lambda = 0.63 \text{ GeV}. \tag{3.7}$$

The results are shown by the solid lines in Fig. 1. Despite its appearance in (3.6) we have made no attempt to favor an integral value for $a+b$. To fit nine moments for both proton and neutron data places rather severe constraints on the parameters. To be able to fit the data so well is in itself an indication of the physical relevance of the model.

Using the same parameters in (3.6) and (3.7) we have calculated the same quantities at $Q^2 = 12.5$ GeV^2. The result together with data are also shown in Fig. 1. Although the agreement is not bad, there are some discrepancies which we have anticipated, since the leading-order approximation is not expected to be good at lower values of Q^2.

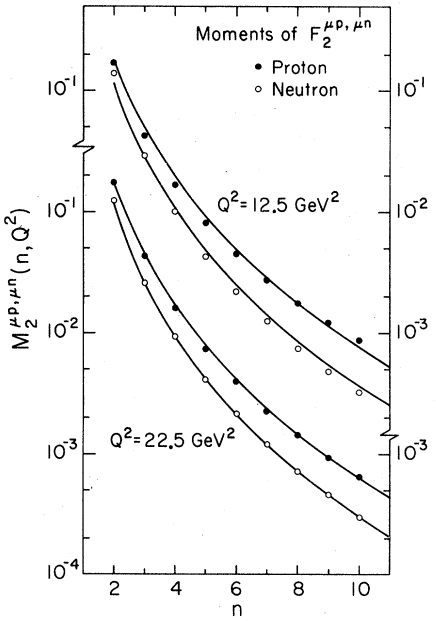

FIG. 1. Moments of $F_2^{\mu p}$ and $F_2^{\mu n}$. Data are from Ref. 14. Valon distributions are adjusted to give best fit to the $Q^2 = 22.5$ GeV^2 data, as shown by the solid lines. The solid lines for $Q^2 = 12.5$ GeV^2 are calculated results using the same distributions.

Thus we go in the other direction and consider neutrino scattering at higher Q^2. First, we note that the parameters obtained in (3.6) and (3.7) pertain to two separate parts of the problem. The parameters a and b describe the valon distributions in a nucleon, while Q_0 and Λ characterize the valon structure in leading-order perturbative QCD. So far we have found[3,4] that the values of Q_0 and Λ vary somewhat according to the experimental data used. It is well known that the data of Aachen-Bonn-CERN-London-Oxford-Saclay (ABCLOS)[17] and CERN-Dotrmund-Heidelberg-Saclay (CDHS)[18] differ not only in the inferred values of Λ, but also in their normalizations. Thus in fitting the neutrino data we allow the values of Q_0 and Λ to deviate from the values given in (3.7) in order to account for a possible mismatch in normalizations. We assume that a and b do not vary from experiment to experiment because they characterize the relationship between moments (hence, insensitive to absolute normalization of the data) while Q_0 and Λ describe the evolution in Q^2 and are more sensitive to the experimental normalization. For the neutrino data we choose the ones provided by the CDHS group,[19] which have far smaller errors quoted than in Ref. 17. The data for M_3 are shown in Fig. 2 for four different values of Q^2. We used (2.21), (2.24), (3.5), and (3.6) to fit the data by adjusting Q_0 and Λ, and found perfect fit for all Q^2 values (es-

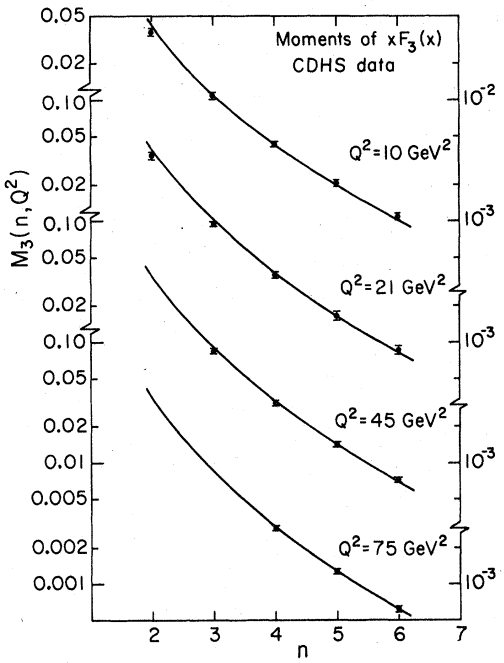

FIG. 2. Moments of $xF_3(x)$. Data are from Ref. 18. The solid lines are calculated results.

pecially high ones) for

$$Q_0 = 0.79 \text{ GeV}, \quad \Lambda = 0.66 \text{ GeV}. \tag{3.8}$$

These values do not differ very much from those in (3.7). Note that the same values of a and b, as specified in (3.6), have been used; we therefore regard them as having been reliably determined. In the following calculations we shall adopt the average values of Q_0 and Λ from (3.7) and (3.8), i.e.,

$$Q_0 = 0.8 \text{ GeV}, \quad \Lambda = 0.65 \text{ GeV}. \tag{3.9}$$

It is fitting to remark here that the value of Λ is determined here phenomenologically and is independent of n. The analysis of Duke and Roberts[14] using lower values of Q^2 yields large errors bars for the values of Λ as a function of n, so much so that they are consistent with both a constant value at $\Lambda = 0.65$ GeV and an n-dependent Λ_n suggested by first-nonleading-order calculations.[11] In fact, a constant value for Λ fits the data better. Theoretically, the value of Λ is meaningless unless the nonleading terms are specified whereupon the n dependence emerges. Even so the normalization of Λ_n must still be determined by experiment. In our model we have ignored the possible n dependence of both Λ and Q_0; if Λ is allowed to depend on n, then Q_0 is likely to depend on n also, but in a way that is unknown at this stage. We have defined Q_0 in the context of leading-order evolution only for which neither Λ nor Q_0 have n dependence and both are to be determined phenomenologically. As long as the values of Λ and Q_0, as given in (3.9), give good fits to the data at high Q^2 in the framework of the valon model, they are useful for the determination of the valon distribution at Q_0 and the quark and gluon distributions at any high Q.

Substituting (3.6) into (3.2) and (3.3) we have the result

$$G_{U/p}(y) = 7.98 y^{0.65}(1-y)^2, \tag{3.10a}$$

$$G_{D/p}(y) = 6.01 y^{0.35}(1-y)^{2.3}. \tag{3.10b}$$

A plot of these functions is shown in Fig. 3(a). If the valons were loosely bound so that their kinetic energies in the nucleon are negligible, then their momentum distributions would be close to $\delta(y - \frac{1}{3})$. The fact that the functions in (3.10) are significantly broader than a δ function at $y = \frac{1}{3}$ signifies that the valons are not loosely bound. They cannot be too tightly bound either, for, otherwise, the impulse approximation implied in (2.1) would be invalid and the model cannot be expected to work as well as it does. The model basically involves only two parameters (a and b) besides Q_0 and Λ and yields good fits to all deep-inelastic scattering data at high Q^2.

It is possible to infer from (3.10) an interesting implication about the matter- and charge-density distributions. These two distributions in the coordinate space have been assumed to be the same in the droplet model of Chou and Yang.[20] The statement to be made here is in the y variable, i.e., the longitudinal-momentum space which is related to the coordinate space by a Fourier transform and a boost to infinite-momentum frame. First, it should be recognized that the matter and charge densities of the valons ought to be independent of the valon flavors,

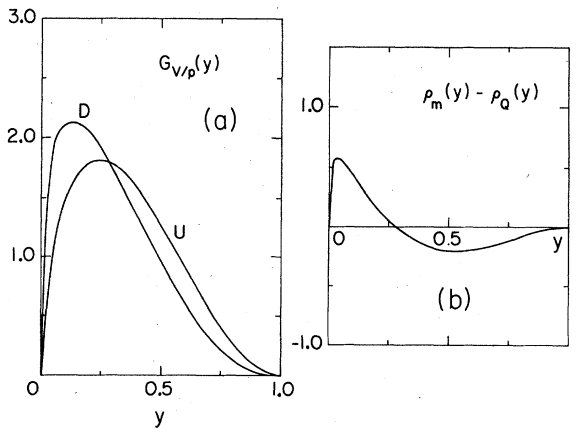

FIG. 3. (a) U and D valon distributions in the proton. (b) Difference between matter-density and charge-density distributions.

since the valon structure is due to QCD virtual processes which are flavor independent. Hence, the charge-density distribution in a proton is

$$\rho_Q(y) = \tfrac{4}{3} G_{U/p}(y) - \tfrac{1}{3} G_{D/p}(y), \tag{3.11}$$

whereas for the matter-density distribution we presume that it is proportional to the total valon distribution, i.e.,

$$\rho_m(y) = \tfrac{1}{3}[2G_{U/p}(y) + G_{D/p}(y)]. \tag{3.12}$$

Both $\rho_Q(y)$ and $\rho_m(y)$ are normalized to one upon integration over y. Evidently, their difference is

$$\rho_m(y) - \rho_Q(y) = \tfrac{2}{3}[G_{D/p}(y) - G_{U/p}(y)], \tag{3.13}$$

which is shown in Fig. 3 (b). Whether this is small enough to be negligible depends upon the model in which this difference enters into the consideration and upon the accuracy demanded.

IV. PARTON DISTRIBUTIONS

Having obtained the valon distributions, the determination of the parton distributions is straightforward. In the following we shall let the number of flavors f increase, as Q^2 is increased. Recall first that the muon data at $Q^2 = 22.5$ GeV^2 have been used as phenomenological input. For such data we have assumed $f = 3$ in the determination of the valon distributions. Starting from the valon distributions we now calculate the parton distributions for both $f = 3$ and 4 at higher Q^2. Of course, how the transition from 3 to 4 takes place, as Q^2 is increased, is hard to ascertain. Threshold effects due to charm quarks cannot be unambiguously introduced. We shall provide a smooth interpolation formula for every quantity that depends on f and Q^2.

The distributions that we shall calculate (all referring to the proton) are for the valence u-quark $xu_v(x)$, valence d quark $xd_v(x)$, sea quarks $xu_{\rm sea}(x) = x\bar{u}(x) = xd_{\rm sea}(x) = x\bar{d}(x) = xs(x) = x\bar{s}(x)\cdots$, generically denoted by $x\bar{q}(x)$, and gluons $xG(x)$. Their moments are denoted, respectively, by $M_{u_v}(n,s)$, $M_{d_v}(n,s)$, $M_{\rm sea}(n,s)$, and $M_g(n,s)$, where s is the evolution parameter. Following the procedure in Sec. II, we obtain

$$M_{u_v}(n,s) = 2U(n) M^{\rm NS}(n,s), \tag{4.1}$$

$$M_{d_v}(n,s) = D(n) M^{\rm NS}(n,s), \tag{4.2}$$

$$M_{\rm sea}(n,s) = (2f)^{-1}[2U(n) + D(n)] \times [M^{\rm S}(n,s) - M^{\rm NS}(n,s)], \tag{4.3}$$

$$M_g(n,s) = [2U(n) + D(n)] M_{gQ}(n,s), \tag{4.4}$$

where M_{gQ} is the quark-to-gluon evolution function given by[13]

$$M_{gQ}(n,s) = \Delta^{-1} d_{gQ}[\exp(-d_+ s) - \exp(-d_- s)]. \tag{4.5}$$

The calculation of these moments is simple. We have used (3.5) and (3.6) for the valon moments and $f = 3$ and 4 in (2.24), (2.25), and (4.5) for a number of values of s between 2.0 and 2.8. Instead of exhibiting the moment distributions, we present the results in parametric form. That is, for every s we fit the moments by a sum of beta functions that are the moments of the following forms for the parton distributions:

$$xq_v(x) = a(1-x)^b x^c,$$

where $q_v(x)$ can be either $u_v(x)$ or $d_v(x)$, and

$$\left.\begin{matrix} x\bar{q}(x) \\ xG(x) \end{matrix}\right\} = \sum_{i=1}^{3} a_i (1-x)^{b_i}. \tag{4.7}$$

Good fits to within 2% of the moments in (4.1)–(4.4) have been achieved with the parameters shown as dots in Figs. 4–7. Almost all the parameters depend on s linearly; the exceptions are b_1 for $x\bar{q}(x)$ and a_3 and b_3 for $xG(x)$. Those that are linear are further parametrized in the following notation:

$$a(s) = a(0) + a's \tag{4.8}$$

with similar expressions for $b(s)$, $c(s)$, $a_i(s)$, and $b_i(s)$. The tabulation of the coefficients $a(0)$, a', etc. in Table I then completely specifies these parameters. For the nonlinear ones the fits are

$$\text{sea: } b_1(s) = \begin{cases} 6.76 - 6.56e^{-s} & (f=3), \\ 6.98 - 6.56e^{-s} & (f=4), \end{cases} \tag{4.9}$$

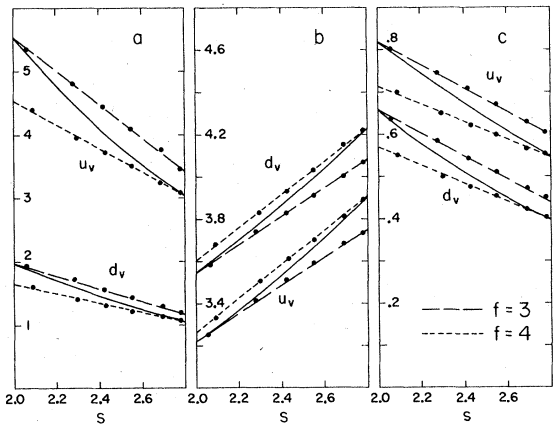

FIG. 4. Parameters a, b, and c in Eq. (4.6) for u and d valence-quark distributions. The dots represent values obtained directly from moment inversion. The broken and dashed lines are straight-line fits of the dots for three and four flavors, respectively. The continuous lines represent interpolations between the two cases of flavors according to the prescription described in the text.

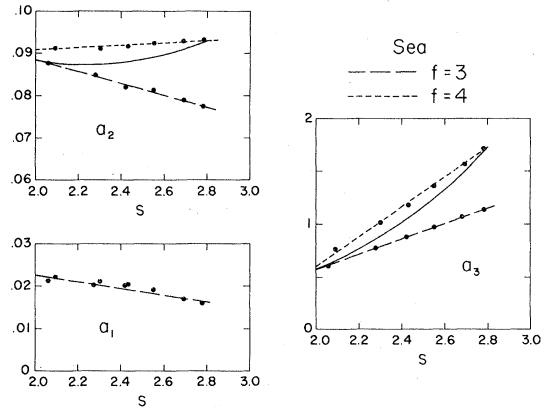

FIG. 5. Parameters a_i in Eq. (4.7) for the sea-quark distribution $x\bar{q}(x)$. Descriptions of the symbols in the figures are as in Fig. 4.

$$\text{glue:}\begin{cases} a_3(s)=\begin{cases}[1+b_3(s)](-0.117+0.164s) & (f=3),\\ [1+b_3(s)](-0.064+0.146s) & (f=4),\end{cases}\\ b_3(s)=\begin{cases}27+4.2e^s & (f=3),\\ 20+6.2e^s & (f=4).\end{cases}\end{cases} \tag{4.10}$$

(4.11)

These fits are represented by the broken ($f=3$) and dashed ($f=4$) lines in Figs. 4–7.

At low Q^2 we expect $f=3$ to be relevant, but at high Q^2 f should be 4. How the transition takes place is complicated and unknown. It seems to us that a smooth interpolation between the two in the description of the parton distribution functions would be useful. There is, of course, no unique way of doing this. We choose a formula in which the incremental change of the parameters is proportional to the change in s. We pin the interpolating parameters to those for $f=3$ at $s=2.0$ and those for $f=4$ at $s=2.8$. Note that the values of Q^2 corresponding to these values of s are, according to (2.2) and (3.9),

$$Q^2(s=2.0)=9.1\ \text{GeV}^2, \tag{4.12a}$$

$$Q^2(s=2.8)=390\ \text{GeV}^2. \tag{4.12b}$$

There is no significance to the precise values of these choices; the reader with alternative preferences can easily make his substitutions. Using $s=2$ and 2.8 for definiteness, we have for the interpolation formula

$$p(s)=p_3(s)+\frac{s-2}{0.8}[p_4(s)-p_3(s)], \tag{4.13}$$

where $p_f(s)$ stands for any one of the parameters $a(s)$, $b(s)$, etc., for flavor f. They are plotted as solid lines in Figs. 4–7. With these interpolating parameters we now have a smooth prediction of all parton distribution functions in accordance to (4.6) and (4.7) for $s>2$. They are shown in Figs. 8 and 9 for various representative values of Q^2. A comparison of the shapes and normalizations of the various parton distributions at $Q^2=100\ \text{GeV}^2$ is shown in Fig. 10.

Several remarks are now in order. First, the large-x behaviors of $u_v(x)$ and $d_v(x)$ are governed by the parameters b in (4.6), and according to Fig. 4 they differ by only 0.3 for all values of s. This is significantly less than the difference of one unit that was guessed by Field and Feynman[21] and subsequently used by many others. Since our result is based on recent data of muon deep-inelastic scattering on neutron and proton having very small error bars, and since we make no guesses, our result should be more reliable.

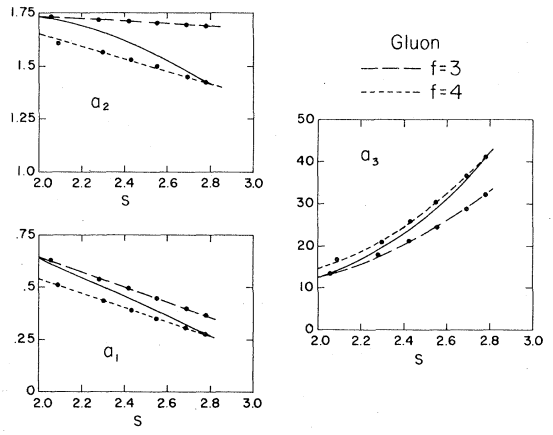

FIG. 6. Parameters a_i in Eq. (4.7) for the gluon distribution $xG(x)$. Descriptions of the symbols in the figures are as in Fig. 4, except that for a_3 the fits are exponential.

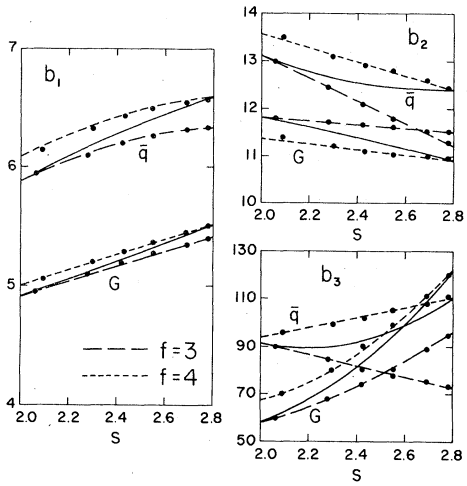

FIG. 7. Parameters b_i in Eq. (4.7) for both sea-quark and gluon distributions. Descriptions of the symbols in the figures are as in Fig. 4, except that b_1 for $x\bar{q}(x)$ and b_3 for $xG(x)$ are nonlinear.

TABLE I. Quark and gluon parameters.

Valence-quark parameters

		a		b		c	
		$a(0)$	a'	$b(0)$	b'	$c(0)$	c'
$f=3$	u_v	10.78	−2.63	1.89	0.66	1.36	−0.27
	d_v	3.96	−1.00	2.22	0.66	1.19	−0.27
$f=4$	u_v	8.28	−1.89	1.66	0.8	1.14	−0.21
	d_v	3.27	−0.8	1.99	0.8	0.98	−0.21

Sea-quark parameters

	$f=3$				$f=4$			
	a_i		b_i		a_i		b_i	
i	$a_i(0)$	a_i'	$b_i(0)$	b_i'	$a_i(0)$	a_i'	$b_i(0)$	b_i'
1	0.044	−0.01	a	a	0.044	−0.01	a	a
2	0.117	−0.01	16.6	−1.5	0.085	0.003	18	−2.44
3	−0.92	0.74	54	20	−2.2	1.4	138.5	−23.75

Gluon parameters

	$f=3$				$f=4$			
	a_i		b_i		a_i		b_i	
i	$a_i(0)$	a_i'	$b_i(0)$	b_i'	$a_i(0)$	a_i'	$b_i(0)$	b_i'
1	1.34	−0.35	3.6	0.65	1.25	−0.35	3.7	0.65
2	1.87	−0.063	12.6	−0.38	2.25	−0.3	12.7	−0.63
3	a	a	a	a	a	a	a	a

[a] See Eqs. (4.10)–(4.12).

Note that the value of b itself for u_v is about 3.2 at $s=2$ and is roughly one unit higher than the exponent of $1-y$ in (3.10a) for the U-valon distribution. This can easily be understood from the basic convolution equation, (2.1), in which $\mathcal{F}^v(z,Q^2)$ approaches a nonvanishing constant as $z\to 1$, if Q^2 is small enough.

The small-x behaviors of $xu_v(x)$ and $xd_v(x)$ are governed by the parameter c, which according to Fig. 4 is around 0.5 for $xd_v(x)$ but higher by almost 0.2 for $xu_v(x)$. The former is roughly consistent with Regge behavior.[22] Note that this is a property that emerges from our analysis and was not put in *a priori* as a boundary condition.

Note also that our results exhibit sharp peaks in both $x\bar{q}(x)$ and $xG(x)$ at very small x. From the parametrizations it is clear that they both approach finite values ($\sim a_3$) at $x=0$, but they are damped very fast [$\sim(1-x)^{b_3}$] as x increases. Essentially, the $i=3$ term in the sum in (4.7) which accounts for this sharp peak contributes only to the $n=2$ moment. This is due to the effectiveness of soft-gluon bremsstrahlung in QCD and has been noted by certain papers in Ref. 10. The large-x behaviors governed by the exponent b_1 shown in Fig. 7 are roughly what one would expect. The

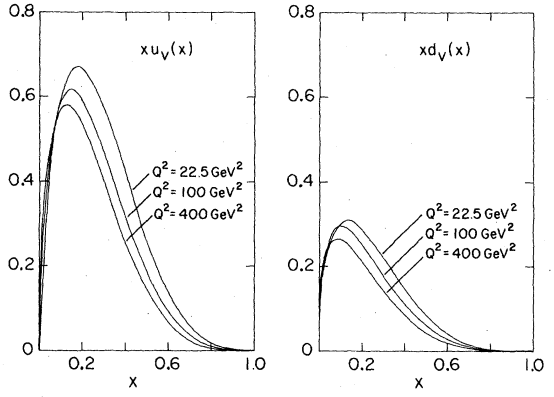

FIG. 8. The distributions of $xu_v(x,Q^2)$ and $xd_v(x,Q^2)$ for various values of Q^2 using interpolated values for the parameters $a(s)$, $b(s)$, and $c(s)$.

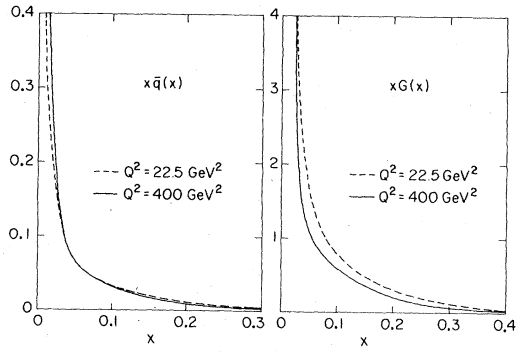

FIG. 9. The distributions of $x\bar{q}(x,Q^2)$ and $xG(x,Q^2)$ for two values of Q^2 using interpolated values for the parameters $a_i(s)$ and $b_i(s)$.

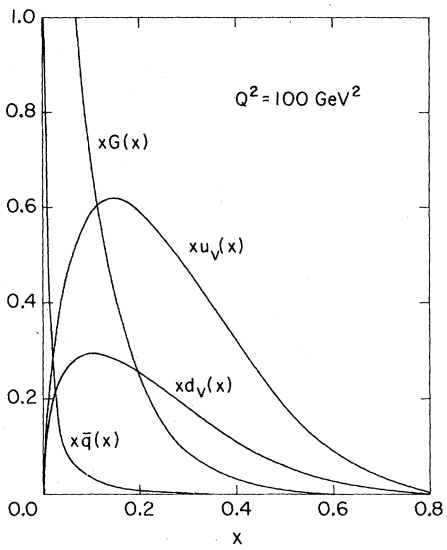

FIG. 10. Plots of $xu_v(x)$, $xd_v(x)$, $x\bar{q}(x)$, and $xG(x)$ for $Q^2 = 100$ GeV^2. The latter two are finite at $x = 0$.

precise behaviors in the limits $x \to 0$ and $x \to 1$ can be examined analytically. In the Appendix we study their behaviors in the framework of QCD and the valon model. The results differ from our parameters in this section, and are applicable only in the extreme limits: $x \ll 0.01$ and $1 - x \ll 0.05$.

In view of the sharp peaks in $x\bar{q}(x)$ and $xG(x)$ at small x, it is of interest to examine the momentum fractions that each of the parton types carries. The average total momentum fraction of each parton type is, of course, the $n = 2$ moment of the appropriate distribution. Now, we have from (4.1)–(4.4) for general n,

$$M_{\rm tot}(n,s) \equiv M_{u_v} + M_{d_v} + 2fM_{\rm sea} + M_g = [2U(n) + D(n)][M^S(n,s) + M_{gQ}(n,s)], \quad (4.14)$$

but in the case $n = 2$ it can be shown that for every fixed f

$$M^S(2,s) + M_{gQ}(2,s) = 1. \quad (4.15)$$

Consequently, on account of (2.16) we also have

$$M_{\rm tot}(2,s) = 1, \quad (4.16)$$

as we should. This is the sum rule that our $n = 2$ moments calculated from (4.6) and (4.7) should satisfy for all s. However, in order to account for the change in f in going from low to high s, (4.13) has been suggested as an interpolating formula for all the parameters $a(s)$, etc. While this procedure provides a smooth evolution for the individual parton distributions, there is no guarantee that (4.16) would be satisfied exactly. The contributions from the four components in (4.14) give

$$M_{\rm tot}(2,s) = \int_0^1 dx\, x[u_v(x,s) + d_v(x,s) + S(x,s) + G(x,s)], \quad (4.17)$$

where

$$S(x,s) = 2f(s)\bar{q}(x,s). \quad (4.18)$$

As with all other parameters, we choose a linear interpolation formula for $f(s)$ from 3 to 4, i.e.,

$$f(s) = 0.5 + 1.25s. \quad (4.19)$$

The four integrated components of (4.17) are shown in Fig. 11. They add up to a sum that satisfies the sum rule (4.16) to an accuracy well within 1% for the entire range of Q^2 plotted. It is therefore reasonable to regard our parametrization as being satisfactory. Now, from Fig. 11 we see that the fraction of momentum that the gluons take is confined to the range from 0.45 to 0.5 which is compatible with earlier guesses and estimates.[21,23] The sharp peak at small x therefore does not imply that the gluons carry an unduly large fraction of the proton momentum. Previous guesses about the x dependences of the gluon and sea-quark distributions are accordingly quite wrong.

To check further the observable consequences of our predictions, we have calculated $F_2(x)$ at $Q^2 = 100$ GeV^2 for muon scattering on nuclear target using $(10s - 8)x\bar{q}(x,s)/9$ as the contribution from all the sea quarks. The result is shown in Fig. 12 where the sharp peak at small x appears as expected. Recent experiment by the European Muon Collaboration (EMC) (Ref. 24) has data at such high Q^2, as shown in the same figure, but only for $x > 0.2$. They agree well with our prediction but are not for sufficiently small x to be able to verify the peak. We have calculated $F_2(x)$ for smaller Q^2 assuming $f = 3$

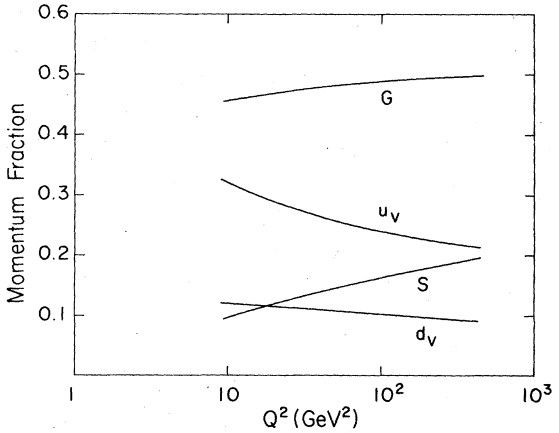

FIG. 11. Total momentum fractions of the four types of partons.

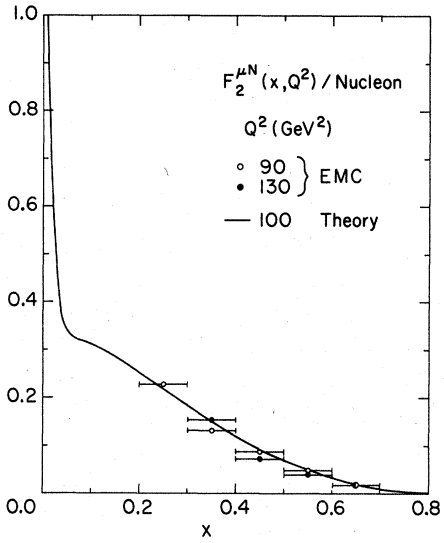

FIG. 12. Structure function for nuclear target at $Q^2 = 100$ GeV^2, calculated using interpolated parameters. Data are from Ref. 22.

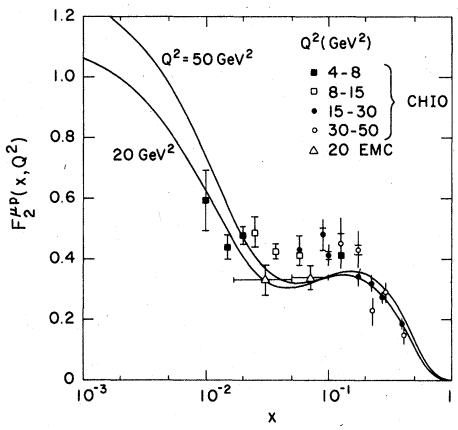

FIG. 13. Structure function for proton at $Q^2 = 20$ and 50 GeV^2, calculated using parameters for $f = 3$. Data are from Refs. 13 and 22.

(without using extrapolation) in the hope of coming closer to the data that exist at extremely small x, but not for such low values of Q^2 as to invalidate our calculation. For $Q^2 = 20$ and 50 GeV^2 the result for μp scattering is shown in Fig. 13. The dip at $x \sim 0.05$ is more prominent than in Fig. 12 because the proton target does not have the smearing effect that exists in the nuclear target for which the dip for the neutron target occurs at a shifted value of x. The CHIO data[15] are generally higher in normalization than those of EMC[24]; the latter has two points that agree perfectly with our prediction. The peaking at extremely small x is hinted by the CHIO data but certainly not verified, especially since the data points are for smaller values of Q^2. Nevertheless, it is encouraging that our prediction at very small x is not ruled out by experiment. It should be remarked, however, that our calculation does not take into account threshold effects associated with massive quarks. At the values of Q^2 shown in Fig. 13, one would expect the charm quarks to exhibit their presence at small x and round out the dip structure.

We have also calculated $F_2^{\mu n}/F_2^{\mu p}$ and $xF_3^{\bar{\nu}p}/F_2^{\bar{\nu}p}$ which are fairly insensitive to Q^2 for $Q^2 > 20$ GeV^2. They are shown in Fig. 14. Data for these ratios are not yet available for the Q^2 range required.

V. CONCLUSION

We have used the valon model to describe deep-inelastic scattering. The model bridges the gap between the bound-state problem and the scattering problem of a hadron. It also eliminates the necessity of making arbitrary guesses about the parton distributions at low Q^2 in the usual theoretical approach to scaling violation. We have determined the valon distributions which now can serve as a goal for the solution of the bound-state problem. From the valon distribution we have further inferred the difference between matter-density and charge-density distributions. Various properties of the nucleon, such as charge radius, high-Q^2 behavior of the form factor, and g_A/g_V, should all be investigated in the light of our knowledge about the nucleon wave function in the valon representation.

We have further calculated the parton distributions at high Q^2 without arbitrary assumptions or parameters, except in the specification of the number of relevant flavors. For both $f = 3$ and 4 we have determined the parameters that describe the x and Q^2 dependences of all the quark and gluon distributions. Formulas are provided for smooth interpolation from $f = 3$ to $f = 4$. The

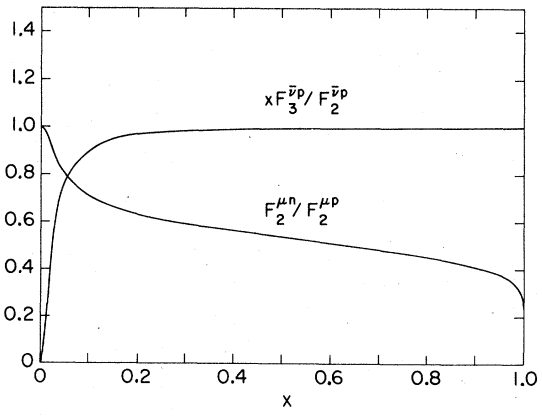

FIG. 14. Ratios of structure functions calculated for $Q^2 = 22.5$ GeV^2, but nearly independent of Q^2.

resultant structure functions agree well with experiment wherever data exist. We predict that a sharp peak and a shoulder should exist at very small x, when Q^2 is large. Experimental verification of this phenomenon would give crucial support to the reliability of the valon model and the applicability of QCD considerations to the problem. As it stands our approach offers a complete description of the parton distributions at high Q^2 without any free parameters.

ACKNOWLEDGMENTS

We are grateful to Dr. E. Gabathuler, Dr. A. Para, Dr. R.G. Roberts, and Dr. W.S.C. Williams for their helpful comments and their willingness to communicate the results of their data analyses before publication, without which this work would have been considerably delayed. The work was supported in part by the U.S. Department of Energy under Contract No. EY-76-S-06-2230, Mod. A008.

APPENDIX: ANALYTIC EXPRESSIONS FOR THE PARTON DISTRIBUTIONS

In our approach to the determination of the parton distributions, once the valon distributions are obtained, the parton distributions are completely calculable in principle. However, the inversion of moments is practical only numerically for the bulk of the x range. Our parametrizations of the distributions in x are not expected to be reliable for x outside the range $0.01 < x < 0.95$. Fortunately, in the extreme limits of $x \to 0$ and $x \to 1$, it is possible to determine their behaviors analytically. It is the purpose of this appendix to supplement the results obtained in the text by deriving analytic expressions of the large- and small-x behaviors.

From the moments $M(n,s)$ that are supposedly known the corresponding parton distribution $G(x,s)$ can be obtained by the inverse Mellin transform

$$G(x,s) = \frac{1}{2\pi i}\int_C dn\, x^{-n} M(n,s)\,, \tag{A1}$$

where the contour C in the complex n plane lies to the right of all the singularities of $M(n,s)$ in n (see Fig. 15). This analytic inversion of the moments over the whole range of x is complicated since it calls for the summing over all the residues of the integral in (A1).[25] However, obtaining leading analytic expressions for $G(x,s)$ at large- and small-x regions is much easier.[13,25] We shall do this separately in the following two subsections.

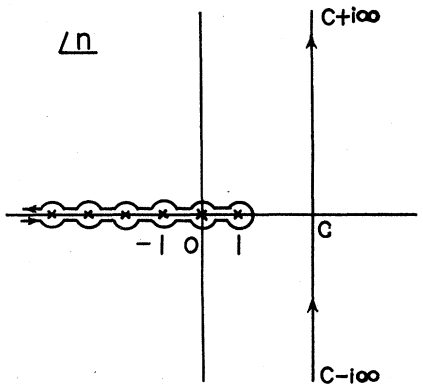

FIG. 15. Contour of integration for integral in (A1).

1. Large-x region ($x \sim 1$)

To obtain analytic expressions in this region it is better to rewrite (A1) as

$$G(x,s) = \frac{1}{2\pi i}\int_C e^{\epsilon n} M(n,s)\,dn\,,$$

where $\epsilon = 1 - x$ and therefore the most dominant behavior at $x \sim 1$ is influenced by the large-n limit of the Mellin transform. In this limit, it can be shown, by using the asymptotic forms of the Γ function, that the U and D valon moments reduce to

$$U(n) = \frac{B(a+n, a+b+2)}{B(a+1, a+b+2)} \sim 15.96 n^{-3}\,,$$

$$D(n) = \frac{B(b+n, 2a+2)}{B(b+1, 2a+2)} \sim 16.13 n^{-3.3}\,.$$

a. Valence-quark distribution

From (4.1) and (4.2) we obtain the expressions for the moments of $u_v(x,s)$ and $d_v(x,s)$, respectively, as

$$M_{u_v}(n,s) = 2U(n)\exp(-d_{NS}s)\,,$$

$$M_{d_v}(n,s) = D(n)\exp(-d_{NS}s)\,.$$

The analytic form for $d_{NS}(n)$ is

$$d_{NS}(n) = \frac{1}{3\pi b}\left\{1 - \frac{2}{n(n+1)} + 4[\gamma_E - 1 + \Psi(n+1)]\right\},$$

where

$$\Psi(n+1) = \Gamma'(n+1)/\Gamma(n+1)$$

$$= \ln(n+1) - \frac{1}{2(n+1)} - \sum_{k=1}^{\infty}\frac{B_{2k}}{2k(n+1)^{2k}}$$

$$= -\gamma_E + \sum_{j=1}^{n}\frac{1}{j} \quad \text{for } n = \text{positive integer}\,.$$

γ_E is the well known Euler constant and its value in $0.577\cdots$ and B_{2k} are the Bernoulli numbers. In the large-n limit we have

$$d_{\rm NS}(n) \underset{n\to\infty}{\sim} -\frac{4}{3\pi b}\left(\tfrac{3}{4}-\gamma_E-\ln n\right)$$

and (A2)

$$M_{u_v}(n,s) \underset{n\to\infty}{\sim} 31.92 n^{-3}\exp\left[\frac{4s}{3\pi b}\left(\tfrac{3}{4}-\gamma_E-\ln n\right)\right],$$

from which, after performing the integration, one derives

$$u_v(x,s) \underset{x\to 1}{\sim} \frac{31.92}{\Gamma(3+4s/3\pi b)} \times\exp\left[\frac{4s}{3\pi b}\left(\frac{3}{4}-\gamma_E\right)\right](1-x)^{2+4s/3\pi b}$$

Proceeding the same way, we obtain for d-valence quark distributions

$$d_v(x,s) \underset{x\to 1}{\sim} \frac{16.13}{\Gamma(3.3+4s/3\pi b)} \times\exp\left[\frac{4s}{3\pi b}\left(\frac{3}{4}-\gamma_E\right)\right](1-x)^{2.3+4s/3\pi b}$$

From Fig. 4(b), we see that the difference in the values of the parameter b for u quark and d quark is also ~0.3 for any number of flavors. Evidently, this difference which is due to the flavor dependence of the valon distribution persists unaltered in the $x\to 1$ limit.

b. Sea-quark distribution

The moments of the sea-quark distribution are given by

$$M_{qS}(n,s)=\frac{1}{2f}[2U(n)+D(n)][M^S(n,s)-M^{\rm NS}(n,s)].$$

$M^S(n,s)$ can be written as

$$M^S(n,s)=\frac{(d_{\rm NS}-d_-)e^{-d_+s}-(d_{\rm NS}-d_+)e^{-d_-s}}{d_+-d_-}\ .$$

For large n, the leading contributions to the anomalous dimensions are

$$\begin{aligned} &d_+ \sim d_{\rm NS}+\delta\ ,\\ &d_- \sim d_{gg}-\delta\ ,\\ &\delta = d_{gQ}d_{Qg}/(d_{\rm NS}-d_{gg})\ ,\\ &d_{gg}\sim -\frac{3}{\pi b}\left(\tfrac{11}{12}-\gamma_E-\ln n\right)+\frac{f}{6\pi b}\ ,\\ &d_{gQ}\sim -\frac{2}{3\pi b n}\ ,\\ &d_{Qg}\sim -\frac{f}{2\pi b n}\ , \end{aligned} \qquad \text{(A3)}$$

hence

$$d_+-d_-\sim -\frac{5}{3\pi b}\ln n\ ,$$

$$\delta\sim -f(5\pi b n^2\ln n)^{-1}\ .$$

The large-n limit of $d_{\rm NS}$ has been obtained before. With the help of (A2) and (A3) we have

$$M^S(n,s)\underset{n\to\infty}{\sim}\exp(-d_+s)=(1-s\delta)\exp(-d_{\rm NS}s)$$

for $s\delta\ll 1$. This assumption is valid for $n\to\infty$ even for sufficiently large Q^2. Therefore, the large-n expression of the moment of sea-quark distribution finally becomes

$$M_{\rm sea}(n,s)\underset{n\to\infty}{\sim} -\frac{s\delta}{2f}\exp(-d_{\rm NS}s)\left(\frac{31.92}{n^3}+\frac{16.13}{n^{3.3}}\right)$$

and the x distribution becomes

$$\bar q(x,s)\underset{x\to 1}{\sim} C_A(1-x)^{4+4s/3\pi b} + C_B(1-x)^{4.3+4s/3\pi b}\ ,$$

where

$$C_A=\frac{3.19s}{\pi b}\left[\Gamma\left(5+\frac{4s}{3\pi b}\right)\right]^{-1}\exp\left[\frac{4s}{3\pi b}\left(\frac{3}{4}-\gamma_E\right)\right],$$

$$C_B=\frac{1.63s}{\pi b}\left[\Gamma\left(5.3+\frac{4s}{3\pi b}\right)\right]^{-1}\exp\left[\frac{4s}{3\pi b}\left(\frac{3}{4}-\gamma_E\right)\right].$$

We have neglected ln ln terms compared to ln$n$. Here we can see that U and D valons make separate contributions to sea-quark distributions.

c. Gluon distribution

The moments $M_g(n,s)$ of gluon distribution are given by

$$M_g(n,s)=[2U(n)+D(n)]M_{gQ}(n,s)\ .$$

With the help of the results in (A3), the large-n behavior of $M_{gQ}(n,s)$ can be easily derived as

$$M_{gQ}(n,s)=d_{gQ}(e^{-d_+s}-e^{-d_-s})/(d_+-d_-) \underset{n\to\infty}{\sim} \tfrac{2}{5}(n\ln n)^{-1}\exp(-d_{\rm NS}s)\ .$$

Therefore, the x distribution is

$$G(x,s)\underset{x\to 1}{\sim} C_U(1-x)^{3+4s/3\pi b}+C_D(1-x)^{3.3+4s/3\pi b}\ ,$$

where

$$C_U=12.77\left[\Gamma\left(4+\frac{4s}{3\pi b}\right)\right]^{-1}\exp\left[\frac{4s}{3\pi b}\left(\frac{3}{4}-\gamma_E\right)\right],$$

$$C_D=6.45\left[\Gamma\left(4.3+\frac{4s}{3\pi b}\right)\right]^{-1}\exp\left[\frac{4s}{3\pi b}\left(\frac{3}{4}-\gamma_E\right)\right],$$

and we neglected again $\ln\ln n$ terms compared to $\ln n$. We can note the power of $(1-x)$ for gluon and sea distributions differs by one unit and this was also obtained for b_1 in parametrizing their respective distributions earlier in the main section (Fig. 7).

2. Small-x region ($x \sim 0$)

For small x the dominant contribution in inverse Mellin transformation comes from the rightmost singularity in the complex n plane. We can rewrite (A1) as

$$xG(x,s) = \frac{1}{2\pi i}\int_C dn\, e^{(n-1)\nu} M(n,s)\,,$$

where $\nu = \ln(1/x) \to \infty$ as $x \to 0$.

a. Valence-quark distribution

We have

$$xu_v(x,s) = \frac{1}{2\pi i}\int_C 2U(n)\exp[(n-1)\nu - d_{\rm NS}\, s\,]dn\,.$$

The rightmost singularity occurs at $n=0$ as can be observed by looking at the expression for $d_{\rm NS}(n)$. Therefore, keeping only the terms nonzero and singular around $n=0$, we get

$$xu_v(x,s) \underset{x\to 0}{\sim} 5.62 e^{-\nu + s/3\pi b}\frac{1}{2\pi i}\int_C \exp\left(n\nu + \frac{2s}{3\pi b n}\right)dn\,.$$

The integration is well known in terms of the Bessel function of second kind and we get

$$xu_v(x,s) \underset{x\to 0}{\sim} 5.62 e^{s/3\pi b} x\left(\frac{8s}{3\pi b\,\ln 1/x}\right)^{1/2} \times I_1\left[\left(8s/3\pi b\,\ln\frac{1}{x}\right)^{1/2}\right].$$

Similarly, we have

$$xd_v(x,s) \underset{x\to 0}{\sim} 7.57 e^{s/3\pi b} x\left(\frac{8s}{3\pi b\,\ln 1/x}\right)^{1/2} \times I_1\left[\left(8s/3\pi b\,\ln\frac{1}{x}\right)^{1/2}\right],$$

where for large arguments, the Bessel function behaves as

$$I_n(y) \sim e^y/(2\pi y)^{1/2}\,.$$

b. Sea-quark and gluon distributions

For sea-quark and gluon distributions, one can show that the rightmost singularity is at $n=1$. Keeping only the singular and nonvanishing parts of the anomalous dimension as before, we get their expressions around $n=1$ as follows:

$$d_{\rm NS} \sim (n-1)/2\pi b\,,$$

$$d_{gQ} \sim -\frac{4}{3\pi b}\left(\frac{1}{n-1} - \frac{9}{16}\right),$$

$$d_{Qg} \sim -\frac{f}{3\pi b}\,,$$

$$d_{gg} \sim -\frac{3}{\pi b(n-1)} + \frac{1}{2\pi b}\left(\frac{11}{2} + \frac{f}{3}\right),$$

$$d_+ \sim -\frac{1}{2\pi b}\left(\frac{6}{n-1} - \frac{\alpha}{2}\right),$$

$$d_- \sim \frac{4f}{27\pi b}\,,$$

where

$$\alpha = 11 + \frac{2f}{27}\,.$$

Hence, we have

$$M^S(n,s) \underset{n\to 1}{\sim} \tfrac{4}{9} e^{-\alpha s/4\pi b}(n-1)\left[\tfrac{1}{9}f - \tfrac{3}{8}(n-1)\right]\exp\frac{3s}{\pi b(n-1)}$$

and from (4.3),

$$x\bar{q}(x,s) + \frac{x}{2f}[u_v(x,s) + d_v(x,s)] \underset{x\to 0}{\sim} e^{-\alpha s/4\pi b}\frac{4fs}{9\pi b\,\ln 1/x} I_2\left[\left(\frac{12s}{\pi b}\ln\frac{1}{x}\right)^{1/2}\right].$$

For gluons $M_{gQ}(n,s)$ behaves in the $n \to 1$ limit as

$$M_{gQ}(n,s) \underset{n\to 1}{\sim} e^{-\alpha s/4\pi b}\,\tfrac{4}{3}\left[1 - \tfrac{9}{16}(n-1)\right]\exp\frac{3s}{\pi b(n-1)}\,.$$

It then follows from (4.4) that

$$xG(x,s) \underset{x\to 0}{\sim} e^{-\alpha s/4\pi b}\,\tfrac{4}{3}(3s/\pi b\,\ln 1/x)^{1/2} \times I_1[2(3s/\pi b\,\ln 1/x)^{1/2}].$$

[1] A. J. Buras and K. J. F. Gaemars, Nucl. Phys. B132, 249 (1978).
[2] J. F. Owens and E. Reya, Phys. Rev. D 17, 3003 (1978).
[3] R. C. Hwa, Phys. Rev. D 22, 759 (1980).
[4] R. C. Hwa, Phys. Rev. D 22, 1593 (1980).
[5] D. Duke and R. G. Roberts, Phys. Lett. 85B, 289 (1979).
[6] A. Gonzalez-Arroyo, C. Lopez, and F. T. Yndurain, Nucl. Phys. B174, 474 (1980).
[7] A. Bialas and A. J. Buras, Phys. Rev. D 21, 1825 (1980).
[8] L. F. Abbott and R. M. Barnett, Ann. Phys. (N.Y.) 125, 276 (1980).
[9] V. Chang and R. C. Hwa, Phys. Rev. Lett. 44, 439 (1979); Phys. Rev. D 23, 728 (1981).
[10] G. Altarelli, N. Cabibbo, L. Maiani, and R. Petronzio, Nucl. Phys. B69, 531 (1974); N. Cabibbo and R. Pet-

ronzio, *ibid.* B137, 395 (1978); T. Kanki, Prog. Theor. Phys. 56, 1885 (1976); A. Bialas, W. Czyz, and W. Furmanski, Acta Phys. Pol. B8, 585 (1977); V. V. Anisovich, Yu. M. Shabelsky, and V. M. Shekhter, Nucl. Phys. B133, 477 (1978); M. Glück and E. Reya, *ibid.* B130, 76 (1977); F. Martin, Phys. Rev. D 19, 1382 (1979); H. Minakata, *ibid.* 20, 1656 (1979).

[11]A. J. Buras, Rev. Mod. Phys. 52, 199 (1980).

[12]We use Cornwall-Norton moments rather than Nachtmann moments because to neglect target-mass effects at high Q^2 is consistent with other approximations adopted in this formalism. Moreover, it makes possible the application of the convolution theorem in (2.13), which is the conerstone of our approach.

[13]T. A. DeGrand, Nucl. Phys. B151, 485 (1979); I. Hinchliffe and C. H. Llewellyn Smith, *ibid.* B128, 93 (1977).

[14]D. Duke and R. G. Roberts, Nucl. Phys. B166, 243 (1980).

[15]B. A. Gordon *et al.* (CHIO Collaboration), Phys. Rev. D 20, 2645 (1979).

[16]A. Bodek *et al.*, Phys. Rev. D 20, 1471 (1979); M. Mertayer *et al.*, Report No. SLAC-Rep-214, 1979 (unpublished); J. S. Poucher *et al.*, Phys. Rev. Lett. 32, 118 (1974); Report No. SLAC-PUB-1309, 1973 (unpublished); W. B. Atwood *et al.*, Phys. Lett. 64B, 479 (1976); Report No. SLAC-185, 1975 (unpublished); E. D. Bloom *et al.*, Report No. SLAC-PUB-653 (unpublished); S. Stein *et al.*, Phys. Rev. D 12, 1884 (1975); G. Miller *et al.*, *ibid.* 5, 528 (1972).

[17]P. C. Bosetti *et al.* (ABCLOS Collaboration), Nucl. Phys. B142, 1 (1978).

[18]J. G. H. deGroot *et al.* (CDHS Collaboration), Z. Phys. C 1, 143 (1979).

[19]A. Para, in *Proceedings of 1979 International Symposium on Lepton and Photon Interactions at High Energy, Fermilab, 1979,* edited by T. B. W. Kirk and H. D. I. Abarbanel (Fermilab, Batavia, Illinois, 1979); also by private communication.

[20]T. T. Chou and C. N. Yang, *High Energy Physics and Nuclear Structure,* edited by G. Alexander (North Holland, Amsterdam, 1967), p. 348; Phys. Rev. 170, 1591 (1968).

[21]R. D. Field and R. P. Feynman, Phys. Rev. D 15, 2590 (1977).

[22]J. Kuti and V. F. Weisskopf, Phys. Rev. D 4, 3418 (1971).

[23]R. P. Feynman, *Photon-Hadron Interactions* (Benjamin, Reading, 1972).

[24]E. Gabathuler, in *Proceedings of the International Conference on High-Energy Physics, Geneva, 1979* (CERN, Geneva, Switzerland, 1979), p. 697.

[25]F. Martin, Phys. Rev. D 19, 1382 (1979).